Mechanism and Machine Theory 135 (2019) 176–191

Contents lists available at ScienceDirect

Mechanism and Machine Theory

journal homepage: www.elsevier.com/locate/mechmachtheory

Research paper

A portable and spring-guided hand exoskeleton for exercising flexion/extension of the fingers

Inseong Jo, Yeongyu Park, Jeongsoo Lee, Joonbum Bae*

Department of Mechanical Engineering, UNIST, Ulsan, Korea

ARTICLE INFO

Article history:
Received 29 November 2018
Revised 25 January 2019
Accepted 4 February 2019
Available online 12 February 2019

Keywords:
Hand exoskeleton
Wearable structure
Continuous passive motion (CPM)
Hand rehabilitation

ABSTRACT

In this paper, we developed a portable and spring-guided hand exoskeleton system for exercising flexion/extension of the fingers. The exoskeleton was designed with a simple structure to aid finger motion with one degree of freedom (DOF). The desired joint trajectory of the exoskeleton was determined based on the user joint ROM and general finger motion obtained by the hand flexion/extension experiments. The design of the linkage structure was optimized to maximally satisfy the desired trajectory. A spring attached to the structure generates the force to guide the fingers toward the desired posture when they deviate from the desired position. We used a finite element method (FEM) to analyze the transmitted moments for MCP and PIP joints. A prototype of the device was fabricated, and the performance of the system was experimentally verified. The experimental results of the finger motion indicated that the proposed system provided good guidance for flexion/extension of the fingers. Furthermore, the results of the force distribution experiment verified that the joint moments by the system are matched to the expected moments by FEM analysis. Thus, the CPM device successfully guided the users fingers along the desired trajectory and distributed the expected moments to the joints.

1. Introduction

As the population ages, the number of people suffering from muscle impairment following a stroke or other nerve disorder is also increasing. Rehabilitation is becoming crucial so that patients can continue to carry out daily tasks [1–3]. As many patients have difficulties exercising their impaired body parts alone, continuous passive motion (CPM) is employed along with physical therapy. CPM reduces the muscle spasticity [4] and activates the sensorimotor cortex in chronic stroke patients [5]. CPM is also helpful for reducing edema following surgery or trauma and for maintaining the range of motion (ROM) and joint flexibility [6–8]. Rehabilitation based on robotic technologies enables repetitive and intensive treatment, in contrast to conventional therapies [6,9,10]. Hence, robotic rehabilitation systems have been actively studied [11,12].

The hand is essential for activities of daily living (ADL), as many of our interactions with the environment and with day-to-day objects are performed via the hand [13–15]. However, the research for the hand typically encounters a number of difficulties due to the intricate mechanical characteristic of hands including their relatively small size, high degrees of freedom (DOFs) and complex structure. To actuate many DOFs in the hand, most hand rehabilitation devices have been

* Corresponding author.
E-mail addresses: isjo@unist.ac.kr (I. Jo), ygpark@unist.ac.kr (Y. Park), galanthus@unist.ac.kr (J. Lee), jbbae@unist.ac.kr (J. Bae).

https://doi.org/10.1016/j.mechmachtheory.2019.02.004
0094-114X/

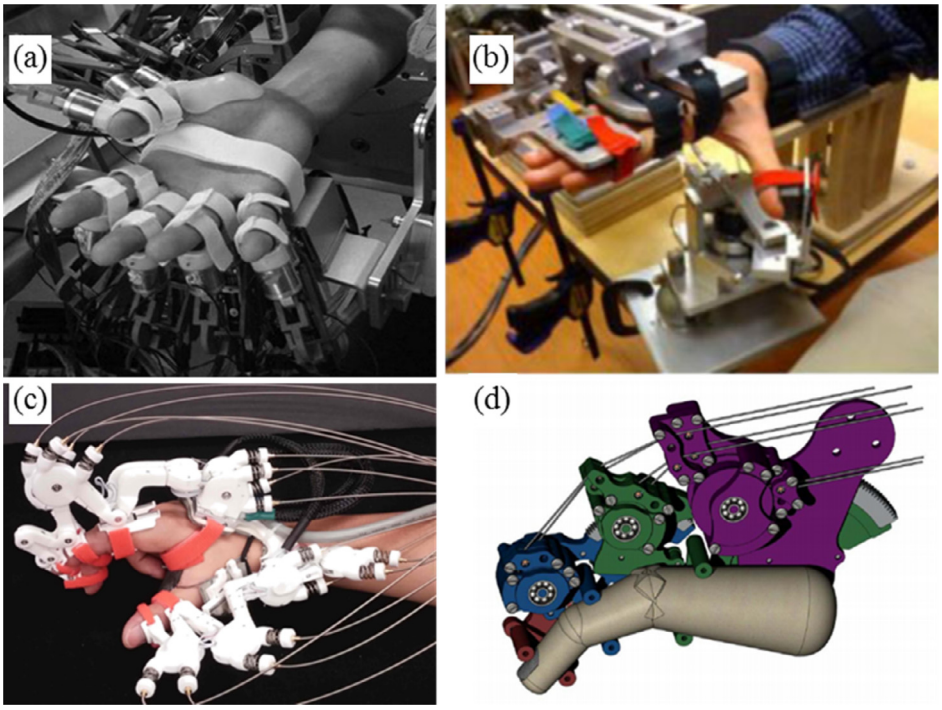

Fig. 1. Previously developed hand rehabilitation systems [17–20].

developed with large numbers of sensors and actuators as shown in Fig. 1 (a) and (b) [16,17]. This enables various finger motions, but typically results in heavy and complex structures. To distribute the weight, these devices have been developed as desk-mounted systems or wrist splint-mounted systems, but the user may feel uncomfortable moving his/her arm when wearing these devices.

To reduce the system size on the hand while maintaining the high DOFs, many hand rehabilitation devices have been developed based on cable-driven mechanisms, as shown in Fig. 1 (c) and (d) [18,19]. The weight of the system on the hand is reduced because the actuators are located on the exterior of the exoskeleton structure. However, cable transmission structures are required alongside the links. This leads to bulky and complex systems. Additionally, externally located actuator modules for cable-driven mechanisms reduce the mobility of the system.

In this paper, we proposed a portable and spring-guided hand exoskeleton for exercising flexion/extension of the fingers. A linkage structure with one degree of freedom (DOF) was designed for exercising four fingers excluding the thumb. General finger motions were obtained from the finger flexion/extension experiment by four subjects. The design of the linkage structure was optimized based on the users hand and joint ROM for comfortable exercises. Also, a spring attached to the structure generates guiding forces for the fingers when they deviated from the desired position. Without a complicated force generation algorithm, the spring acts as a physical impedance and the system can generate the forces for finger exercise. The system performance for finger motions and force distribution by the spring was verified by experiments.

The work presented in this paper is organized as follows. In Section 2, we describe the design of the hand exoskeleton structure. The optimized design of the exoskeleton structure and spring mechanism is explained in Section 3. The system prototype is explained, and, the performance of the exoskeleton with respect to finger motions and force distribution is validated in Section 4. Our conclusions are discussed in Section 5.

2. Design of the hand exoskeleton design

The hand exoskeleton was developed to help exercise the flexion/extension capabilities of the fingers. Generally, each finger, excluding the thumb, have 4 DOFs (1 DOF of abduction/adduction and 3 DOFs of flexion/extension). We reduced the size of the system by omitting consideration of the abduction/adduction motions of the fingers. Also, because the distal interphalangeal (DIP) joint is dependent on the proximal interphalangeal (PIP) joint, we only considered the metacarpophalangeal (MCP) and PIP joints. The exoskeleton is driven by a single motor to ensure that the system is simple. Therefore, we designed the structure to allow natural finger motions with one active joint.

Fig. 2(a) shows how the two rotational joints of the finger are moved by the linkage structure. The designs of the links connecting the finger to the exoskeleton are shown in Fig. 2(b). The structure of the exoskeleton is controlled by the linear motor located on the back of the hand. Each combination of phalanx and connecting link forms a triangular plane, and

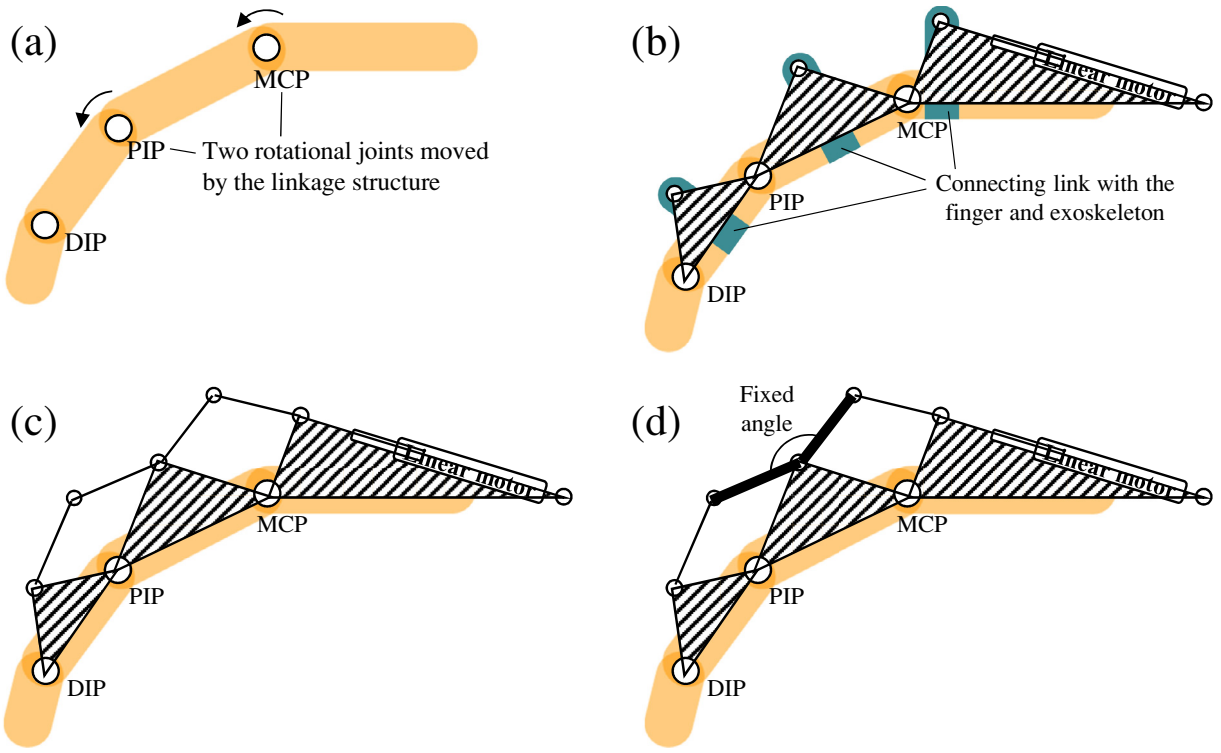

Fig. 2. Proposed kinematic design.

the rotations of these planes cause the finger joint to rotate. We introduced four links and two rotational joints to control the joint angles using the four-bar linkage mechanism shown in Fig. 2(c). With this design, the MCP and PIP joints are controlled independently, as it is impossible to control the finger joints uniquely using a single actuator. Thus, we fixed the angle created by the two four-bar linkages so that the movement of the PIP corresponded to that of the MCP joint, as shown in Fig. 2(d). This design produces natural flexion/extension motions with 1 DOF in the active joint because the resulting structure consists of two linkages involving the MCP and PIP joints.

Fig. 3 shows the proposed design, which is composed of two four-bar linkages (shown in green and blue linkages). The green and blue links determine the angles of the MCP and PIP joints, respectively. Because both the green and blue links are connected to a bent link with three rotational joints, the PIP joint is flexed when the MCP joint is flexed. The green link moves as the length of the motor stroke increases, which in turn affects the movement of the blue links. Because the four-bar linkages are combined with the bent link, the movement of the motor stroke controls the MCP and PIP joint angles simultaneously.

3. Optimized design of the exoskeleton structure

3.1. Hand flexion/extension experiments

The goal of this effort was to enable patients to exercise their impaired hands using the exoskeleton structure. Thus, during the exoskeleton design process, it was important to determine how to make the user's finger move naturally.

We reviewed previous studies on finger motions to investigate a comfortable trajectory for finger flexion/extension. Kamper et al. studied fingertip trajectories during grasping objects [21]. They found that the DIP joint angle varied linearly with the PIP joint angle, but there was no characteristic relationship between the MCP and PIP joint angles. Conti et al. measured a normal person's finger joint trajectories and developed a hand exoskeleton that follows the measured motions [22]. Yang et al. studied a tendon-driven finger exoskeleton based on finger motion coupling [23]. They captured the joint angles of a normal person's index finger and investigated the relationship between the angles of the MCP and PIP joints during hand flexion/extension motions.

Since the fingers should adapt to the object's size or shape during grasping objects, it is difficult to find the relation between MCP and PIP joint angles. In addition, as the finger motions by many people are various according to the individual habits, many researchers have focused on the one person's finger trajectory. However, it is difficult to know whether this movement is applicable to others. Thus, in this paper, we evaluated hand flexion/extension in numerous people to determine the general relationship between the angles of the MCP and PIP joints. To reduce the impact of individual features of

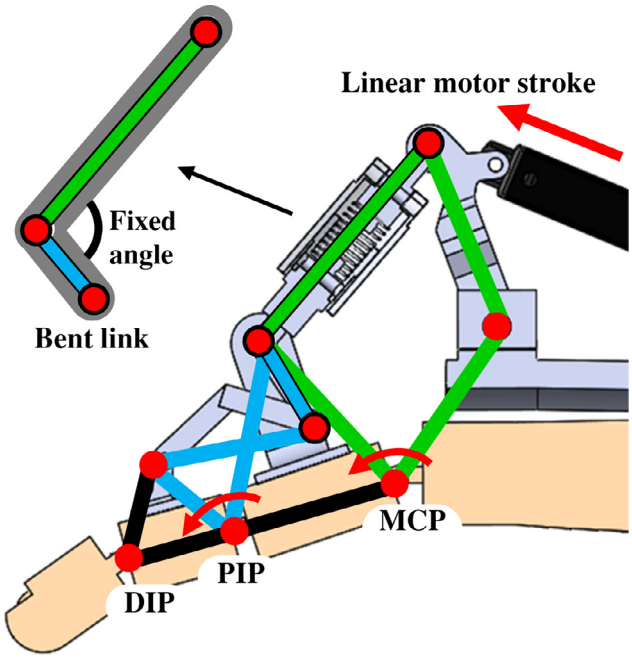

Fig. 3. Kinematic scheme of the proposed structure.

Table 1
Range of motion (ROM) obtained in the experiment.

Joint	Range of motion (ROM)
MCP (°)	0–70
PIP (°)	0–106

grasping motions, subjects followed the hand flexion/extension instructions described in Fig. 4(a). There are three hand postures: flexion, relaxed hand, and extension. The relaxed hand has a partially flexed posture, which is induced by the passive recoil force generated by the flexor digitorum profundus [24]. As shown in the instructions, the subject relaxed his/her hand from the flexion posture and used minimal force to move their fingers into the extension posture. By contrast, the subject with an extended hand relaxed his/her hand, then moved the hand into a flexion posture. By using the minimum force and natural contraction of the fingers, the potential for idiosyncratic motions was minimized. Hence, we captured the general characteristics of finger motions.

In total, four subjects (aged: 25.3 ± 1.71 years) participated in the hand flexion/extension experiment. Markers were attached to the joints of subjects's right index fingers, and they proceeded to flex/relex/extend their hands for 1 min per trial, followed by a 1-min rest between trials. There were three trials in total. The angles of the finger joints were calculated using the positions of the markers, which were measured using a motion capture system (Prime 13, Optitrack, USA). All experiments were conducted with the approval of the institutional internal review board (IRB) (IRB approval number: UNISTIRB-17-23-A).

Fig. 4(b) shows the results of the experiment for each of the subjects' MCP and PIP joint angles. The black dots indicate the angles of the joints for each subject. The finger motion data followed curvilinear trends, which some deviation. The red line shows the polynomial curve that we fitted to the experimental data. The equation for the fitted polynomial was as follows:

$$y = -0.0004239x^3 + 0.0392x^2 + 0.8507x \tag{1}$$

where x and y represent the angles of the MCP and PIP joint, respectively. The range of motion (ROM) data are summarized in Table 1.

3.2. Optimization of the exoskeleton structure

We based our design on the relationships between the joints. However, we needed to reconsider the joint ROM because the CPM device should satisfy the full ROM of the user [8]. We adjusted the equation to satisfy each user's individual ROM while maintaining the relationship between the joint angles.

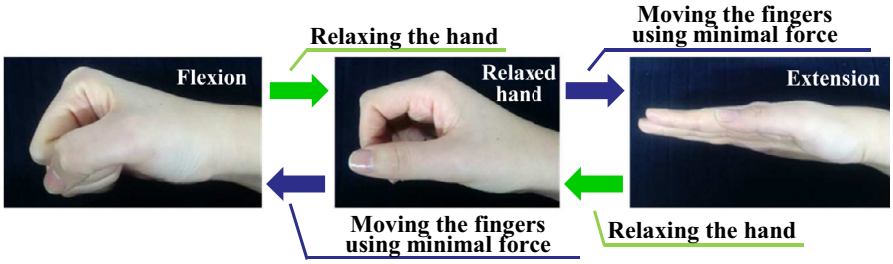

(a) Instructions for hand flexion/extension

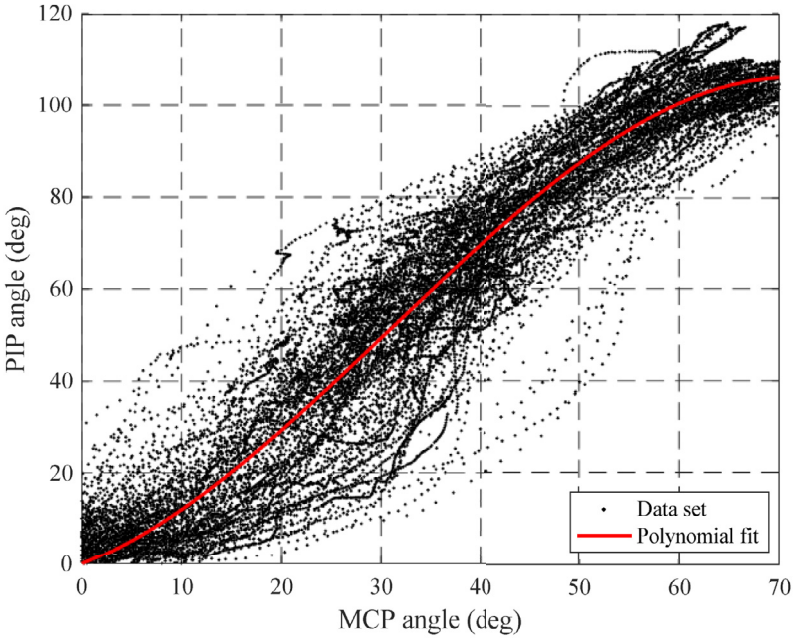

(b) Relationship between MCP and PIP joint angles

Fig. 4. Hand flexion/extension experiments.

Table 2
User information.

Index finger	Length(mm)	Proximal phalanx	40
		Middle phalanx	24
	Range of motion (°)	MCP joint	0–60
		PIP joint	0–90

The polynomial fit was revised by multiplying the joint angles by the ratio between the maximum ROM according to the experimental results and the user's maximum ROM. The adjusted MCP and PIP joint angles were expressed as x' and y', respectively. Thus, we transformed the angle variables as follows:

$$x = \frac{X}{X'}x', \quad y = \frac{Y}{Y'}y' \tag{2}$$

where X and Y represent the maximum MCP and PIP joint angles, respectively, according to the polynomial fitting, and X' and Y' represent the user's maximum MCP and PIP joint angles, respectively. We calculated the equation of the adjusted polynomial fit by substituting (2) to (1).

The user data for the finger are summarized in Table 2. We adjusted the polynomial fit because the maximum MCP and PIP joint angles were 60° and 90°, respectively, as shown in Fig. 5. We used the adjusted equation to calculate the ROM of each individual joint to design a suitable exoskeleton for each user.

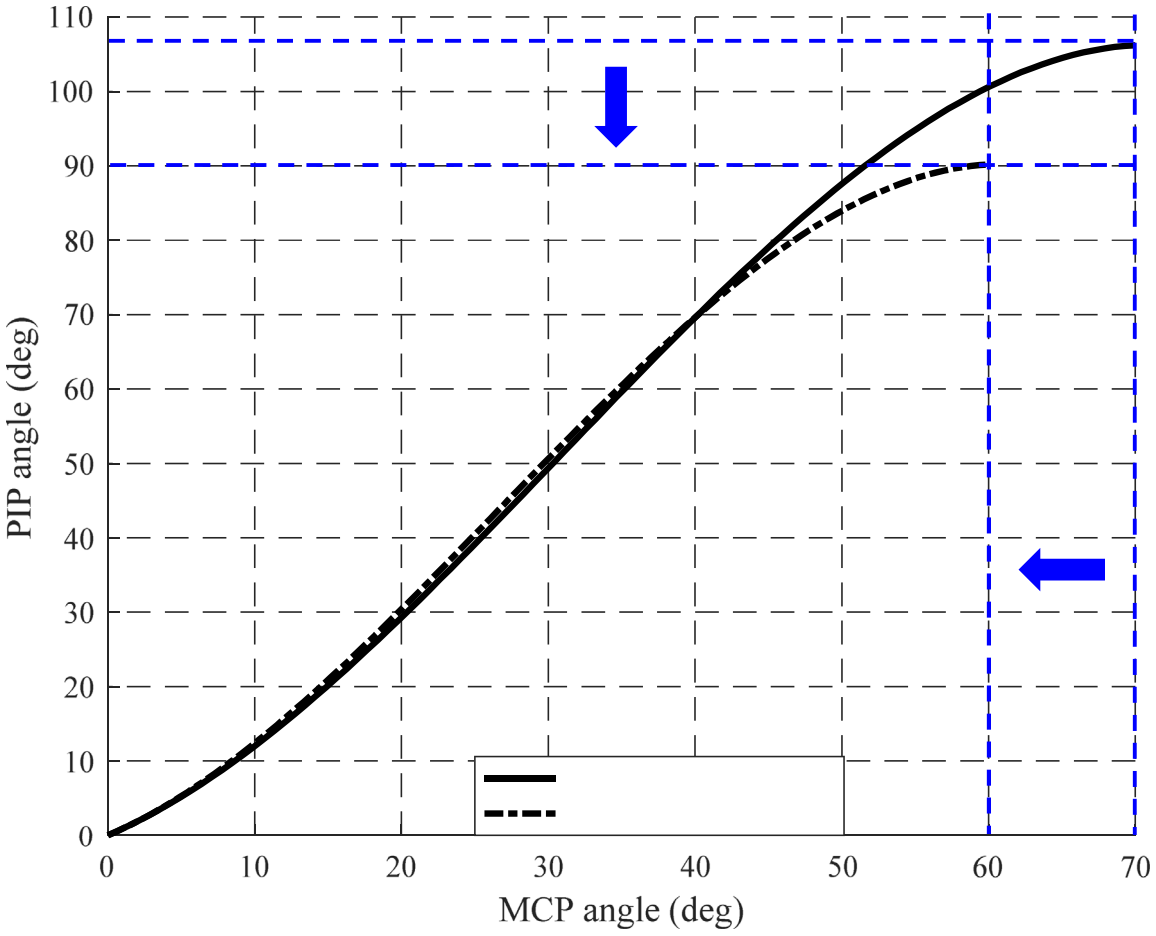

Fig. 5. Adjusted joint relationship.

When the exoskeleton is worn, the finger motions should faithfully replicate the desired finger motions, as specified by the adjusted equation. Thus, it was required to develop an optimization algorithm for the exoskeleton.

Fig. 6 shows the design variables of the proposed exoskeleton structure. l_p and l_m are the lengths of the user's finger phalanges, expressed in Table 2, and l_{act} is the stroke length of the linear motor. There were 14 link-length parameters ($l_1 \sim l_{11}, l_b$) and 5 angle parameters ($\alpha \sim \epsilon$); however, we used 9 independent variables in the optimization algorithm because we excluded the predefined or dependent parameters. The design variable vector for the optimization algorithm was defined as follows:

$$l_i = [l_2 \quad l_4 \quad l_5 \quad l_6 \quad l_7 \quad l_b \quad l_{11} \quad \alpha \quad \varepsilon] \tag{3}$$

Through the optimization algorithm, the l_i vector that generates the motion most similar to the desired motions is selected. The difference between the desired finger motions and the motions generated by the exoskeleton is expressed as a cost function. Here, x_1 is the angle of the MCP joint induced by the exoskeleton as a function of the motor stroke length l_{act}, and y_1 and r_1 are the angles of the PIP joint induced by the exoskeleton and the desired PIP joint angle, respectively. These variables were expressed as functions of the design variable vector l_i and the motor stroke length l_{act} as follows:

$$\begin{aligned} x_1 &= f_{MCP}(l_i, l_{act}) \\ &= \beta + \arccos\left(\frac{l_p}{2l_4}\right) + \arctan\left(\frac{l_2 \sin\psi}{l_1 + l_2\cos\psi}\right) \\ &\quad - \arccos\left(\frac{l_1^2 + l_2^2 + l_4^2 - l_3^2 + 2l_1 l_2 \cos\psi}{2l_4\sqrt{l_1^2 + l_2^2 + 2l_1 l_2 \cos\psi}}\right) - \pi \end{aligned} \tag{4}$$

$$y_1 = f_{PIP}(l_i, l_{act})$$

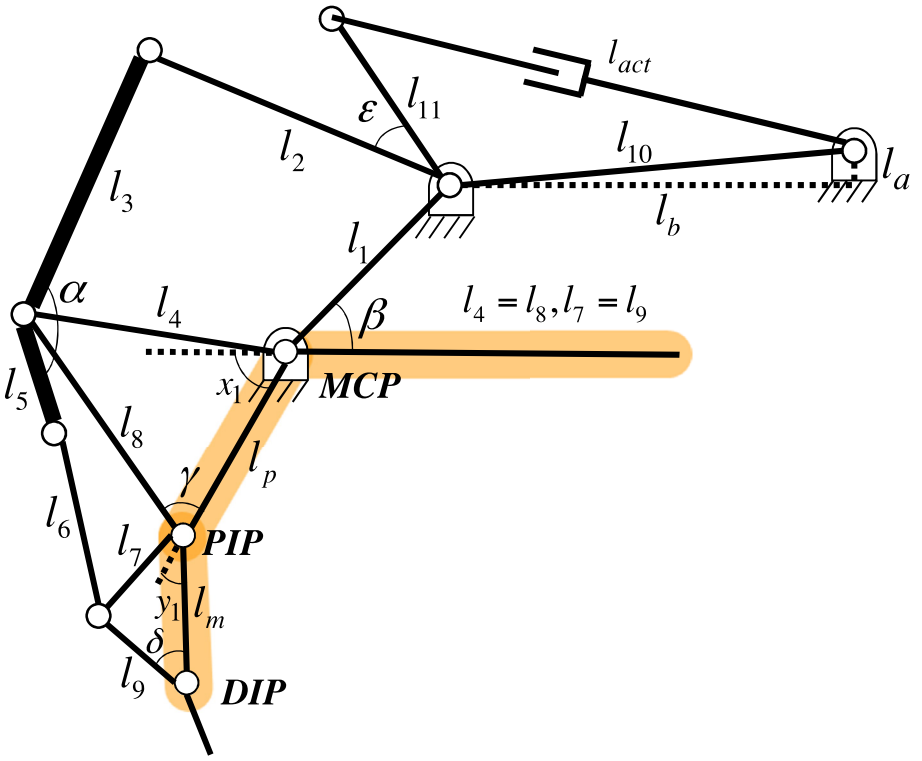

Fig. 6. Parameters considered when designing the exoskeleton system.

$$= \arccos\left(\frac{l_m}{2l_7}\right) + \arccos\left(\frac{l_p}{2l_4}\right) + \arctan\left(\frac{l_5 sin\omega}{l_8 + l_5 cos\omega}\right) + \arccos\left(\frac{l_8^2 + l_5^2 + l_7^2 - l_6^2 + 2l_8 l_5 \cos\omega}{2l_7\sqrt{l_8^2 + l_5^2 + 2l_8 l_5 \cos\omega}}\right) - \pi \tag{5}$$

$$r_1 = g(x_1) = -0.0004239x_1^3 + 0.0392x_1^2 + 0.8507x_1 \tag{6}$$

where f_{MCP} and f_{PIP} are the motion-generation functions for the structure, and g is the function that produces the desired motion. The angles ψ and ω in these equations were calculated as follows:

$$\psi = \epsilon - \beta + \arccos\left(\frac{l_{10}}{l_b}\right) + \arccos\left(\frac{l_{10}^2 + l_{11}^2 - l_{act}^2}{2l_{10}l_{11}}\right) \tag{7}$$

$$\omega = 2\gamma - \alpha + \arccos\left(\frac{l_1^2 + l_2^2 - l_3^2 - l_4^2 + 2l_1 l_2 \cos\psi}{2l_3 l_4}\right) \tag{8}$$

The joint ROM is also an important factor for determining finger motion. y_2 and r_2 are the ROM of the PIP joint while using the exoskeleton and the desired ROM, respectively. These variables also affect the cost function.

$$y_2 = [\min(y_1) \ \ \max(y_1)] \tag{9}$$

$$r_2 = [\min(r_1) \ \ \max(r_1)] \tag{10}$$

Thus, the difference between the joint angles generated by the design variables and those of the desired motions is expressed as the cost function as follows:

$$y = [y_1 \ y_2]^T \tag{11}$$

$$r = [r_1 \ r_2]^T \tag{12}$$

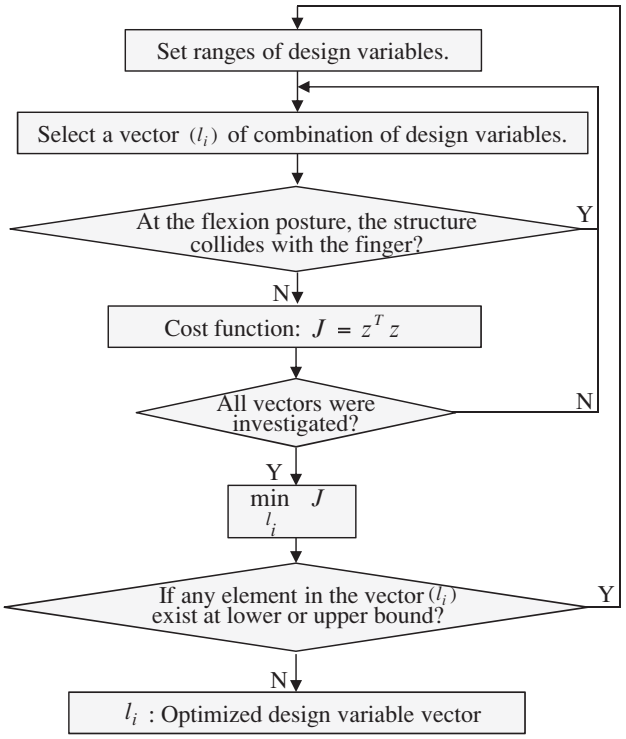

Fig. 7. Flowchart of the optimization algorithm.

Table 3
The optimized design vector.

Variable	l_2	l_4	l_5	l_6	l_7	l_b	l_{11}	α	ϵ
Value	66 mm	54 mm	35 mm	39 mm	23 mm	93 mm	34 mm	132°	33°

$$z = [w_1 \ w_2][y - r] \tag{13}$$

$$J = z^T z \tag{14}$$

where w_1 and w_2 are weights for the relationships between joints and the ROM, respectively, and J is the cost function of the design variable vector. The optimized design for maximally satisfying the desired motions was obtained by finding the design variable vector with the minimum cost.

Fig. 7 shows the process of the optimization algorithm. The optimized design variable vector was obtained through a numerical method because the cost function is a multivariate nonlinear function. If the finger structure by the selected design vector collides with the finger, the design variable vector was selected again. Since the collision occurs when the finger is the most flexed, the finger structure in only flexion posture was checked. If the structure does not collide with the finger, the cost function was calculated. After investigating all variable vectors, the design variable vector with the minimum cost was selected as the optimized design. If any of the elements of the vector was at the lower or upper bound of this motion, the ranges of the design variables were adjusted, and the optimization process was performed again to obtain an optimized vector with a locally minimal cost.

Table 3 describes the optimized design vector. The ratio of l_2 and l_{11} connected to the same joint is important to generate full ROM with the limited motor stroke l_{act}. Thus, the l_2 value was determined to be about twice the l_{11} value to satisfy the wide ROM of the joints with a small motor stroke (30 mm). In addition, since the length of the proximal phalanx is 1.7 times longer thanthat of the middle phalanx, the link l_5, l_6, and l_7 forming 4-bar linkage around the PIP joint are smaller than the link l_2 and l_4 around MCP joint. The determined length of l_b is 93 mm which can be put on the back of the hand. The angle α and ϵ affects to the relation between MCP and PIP joint angle and the starting angle of the MCP joint, respectively. These angles were determined to maximally satisfy the desired joint relation and ROM.

The finger motions obtained by the optimized exoskeleton structure are shown in Fig. 8. The line with stars is the desired finger motion, and the line with dots is the joint angle obtained using the optimized exoskeleton structure. The finger

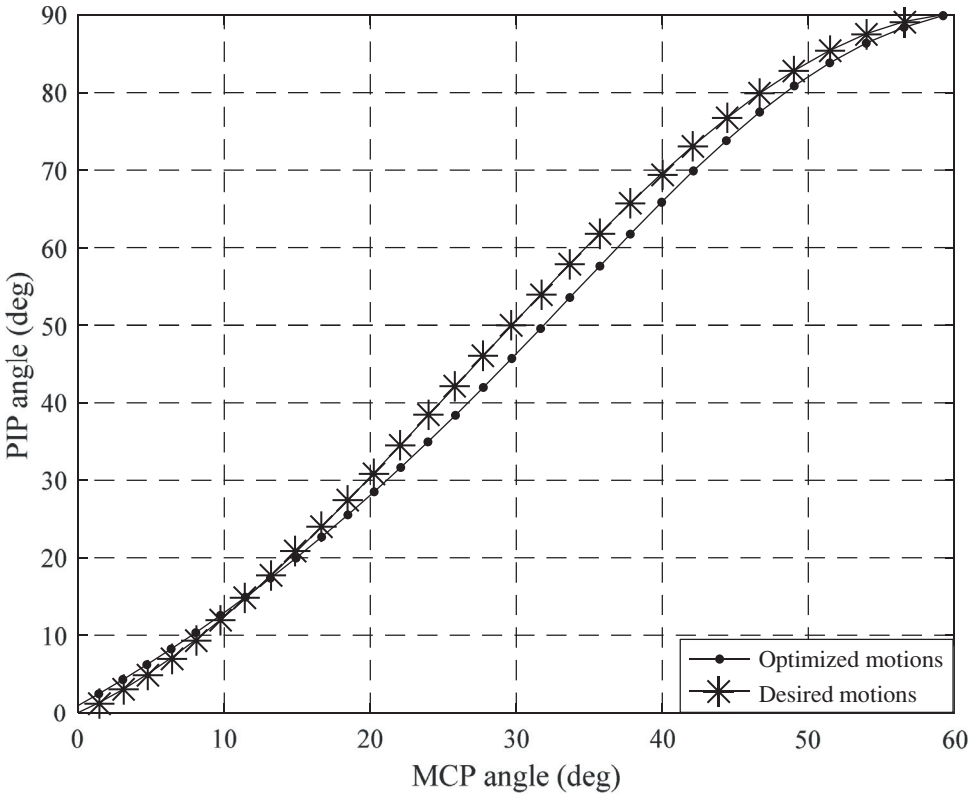

Fig. 8. Optimized finger motions.

motions generated by the exoskeleton were very similar to the desired motions. This indicates that the optimized structure with 1 DOF can guide general finger motions well. This design process enabled us to optimize the hand rehabilitation device, thus enabling the user to carry out flexion/extension exercises for the fingers.

3.3. Spring mechanism

Many hand rehabilitation systems force the fingers to follow a given trajectory; this is the case with continuous passive motion (CPM) devices [17,25]. However, as intended users of the device have problems with moving their fingers freely, guidance systems based on impedance control are better than those based on position control. Thus, we installed a spring to provide the proposed system with passive impedance; the spring force served to guide the finger when the finger deviated from the desired posture. This guidance forces can be generated by the spring installed in the exoskeleton structure without the need for a complex force generation algorithm.

We attached a spring to the bend link, as shown in Fig. 9(a). The spring is compressed when the user extends the finger farther than desired posture. Thus, a spring force is generated in the direction of extension, causing the finger to return to the desired posture. Rather than requiring a large torque sensor, the guiding force is calculated by a potentiometer that measures the spring deflection.

The application of the spring force is determined by how far the finger deviates from the desired posture. Because the amount of spring force by given deflection is dependent on the spring constant, we needed to determine the appropriate value for the spring constant. The spring component of the exoskeleton structure was designed to generate a maximum force of 12 N when the MCP and PIP joint angles deviated from the desired joint angles, by averages of 5° and 15°, respectively. Depending on the patient's condition, the spring constant of the device can be adjusted by replacing it with another spring.

Fig. 9(b) shows finger postures as a function of spring deflection. The line-patterned area indicates finger postures allowed by the proposed structure. The line with the stars shows the finger postures adopted when wearing the exoskeleton structure if the spring is at its normal length. The lines with the circles and dots are the finger postures adopted when the spring is fully compressed and fully stretched, respectively. The finger is guided along the line patterns (in the direction of the red arrow) so that it returns to its intended posture upon deviating from its desired trajectory.

Physically, the spring mechanism can be considered as an impedance control mechanism [26]. One of the most widely known methods for calculating impedance is in terms of the potential field, and the gradient of the potential field can be considered as the impedance [11,27]. Hence, we calculated the potential field representing the spring force around the

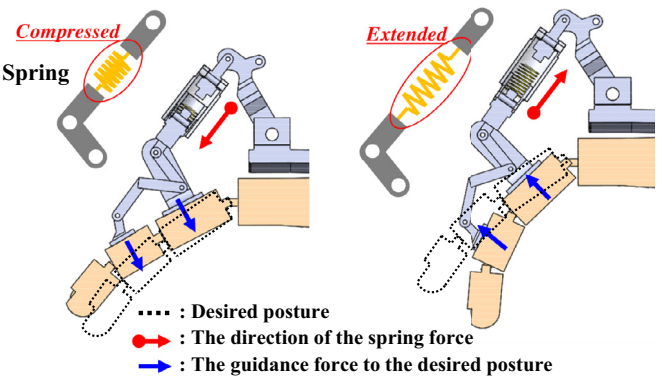

(a) Spring force

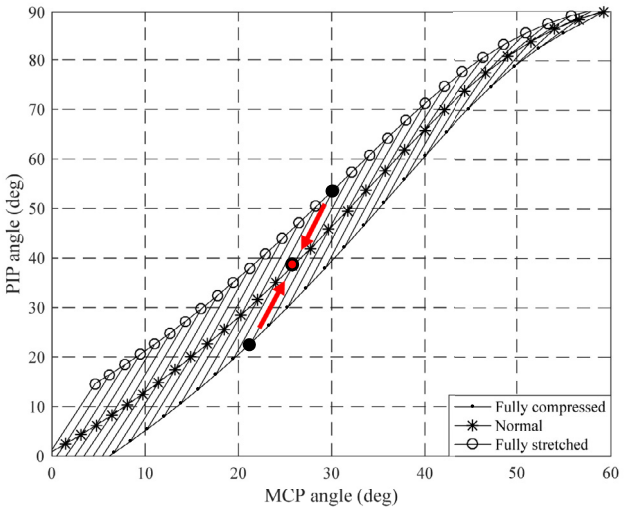

(b) Finger joint angles

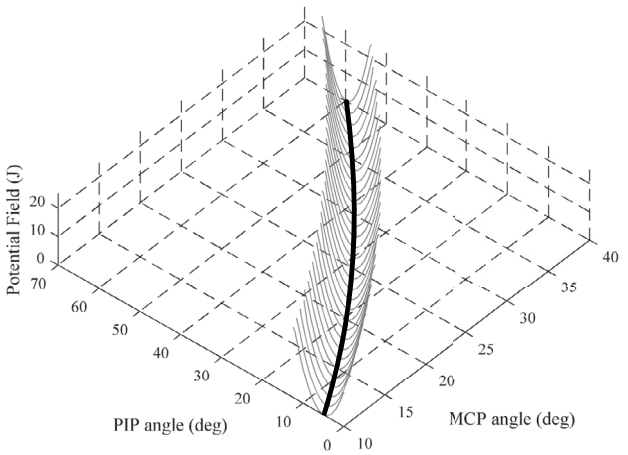

(c) Potential field (thick line: desired joint trajectory, gray lines: potential field)

Fig. 9. Spring mechanism.

desired joint trajectory. Assume that x_H is the end-point of the spring determined by the human finger posture and x_M is the end-point of the spring calculated by the motor stroke length. The potential field was defined as a quadratic function of the difference between x_H and x_M as follows:

$$P = \frac{1}{2}k(x_H - x_M)^2 \tag{15}$$

where k is the parameter of the quadratic function. The impedance force, F, based on the potential field defined in (16) is calculated by differentiating (15), as follows:

$$F = -k(x_H - x_M) \tag{16}$$

The parameter k can be interpreted as a spring constant. The negative sign means that the user feels the spring force in the direction opposite to the deviation in the motion. Fig. 9(c) shows the potential field for the spring force; we have enlarged the section where the MCP joint angle is 10–40° for clear expression. As the position of the finger deviates from its desired posture, the guidance force increases depending on the gradient of the potential field.

The magnitude of the spring force transmitted to each finger joint is proportional to the deviation of the finger. Thus, we analyzed the distribution of the force to determine how the spring force is divided between finger joints. Fig. 10(a) shows a free body diagram of the finger structure. The force generated by the spring is defined as F_s, and the force applied to each rotation joint is F_n. We also indicate the five links required for the analysis of force distribution. The moments transmitted to the MCP and PIP joints are denoted as M_{MCP} and M_{MCP}, respectively.

Since the finger structure includes an indeterminate linkage, we analyzed the force distribution using the finite element method (FEM). We derived the finite element equations based on the principle of minimum potential energy [28]. The spring force is determined by the spring constant and the deflection length. The equation was derived from (16). The links in the finger structure are expressed as stiff bodies that depend on the Young's modulus (E), cross-sectional area (A), length (L), and moment of inertia (I). The variation in the displacement (u, v) and slope (q) of the joint by the distributed forces was calculated using the following equations:

$$[K][Q] = [F] \tag{17}$$

where K is the stiffness matrix of the links, Q is the displacement vector of joints, and F is the force vector. Each matrix can be expressed as follows:

$$K = [f(E, A_i, I_i, L_i)], \quad i : structure\ link \tag{18}$$

$$Q = [u_j v_j q_j \ldots]^T, \quad j : rotation\ joint \tag{19}$$

$$F = [F_s\ F_u]^T \tag{20}$$

where F_s is the spring force, and F_u is the unknown force transmitted to the joints. We introduce the matrix M to combine all of the unknown variables (unknown displacements (Q) and forces (F_u)) into one vector, and then solve the resulting equations using linear algebra. Thus, the above equation can be rewritten as follows:

$$\begin{bmatrix} K & M \end{bmatrix} \begin{bmatrix} Q \\ F_u \end{bmatrix} = \begin{bmatrix} F_s \\ 0 \end{bmatrix} \tag{21}$$

$$\begin{bmatrix} Q \\ F_u \end{bmatrix} = \begin{bmatrix} K & M \end{bmatrix}^{-1} \begin{bmatrix} F_s \\ 0 \end{bmatrix} \tag{22}$$

We used these equations to calculate the unknown displacements and forces. We also calculated the moments of the finger joints based on the forces transmitted to the joints as follows:

$$\overrightarrow{M_{MCP}} = \overrightarrow{l_{10\to 1}} \times \overrightarrow{F_{10}} \tag{23}$$

$$\overrightarrow{M_{PIP}} = \overrightarrow{l_{11\to 7}} \times \overrightarrow{F_{11}} \tag{24}$$

The distributed moments were affected by both the lengths and the cross-sections of the links. We evaluated the effect of the cross-sectional area of the links on the force distribution, by calculating the sensitivity of the moment of the joint to the area. The sensitivity of joint moment means the change in joint moment due to the change in cross-sectional area of each link and it can be calculated as follows:

$$S_{M,A_n} = \frac{\triangle M/M}{\triangle A_n/A_n} \tag{25}$$

where M is the moment of the joint, and A_n is the cross-sectional area of link n.

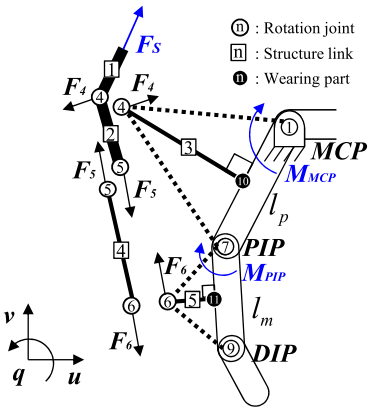

(a) Free body diagram

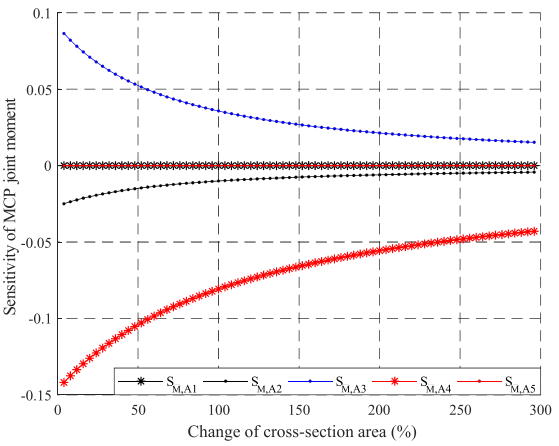

(b) Sensitivity of the force at MCP joint (A_n: Cross-section area of link n)

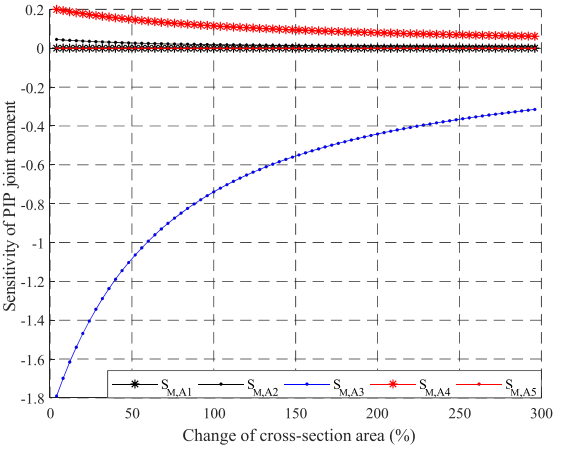

(c) Sensitivity of the force at PIP joint

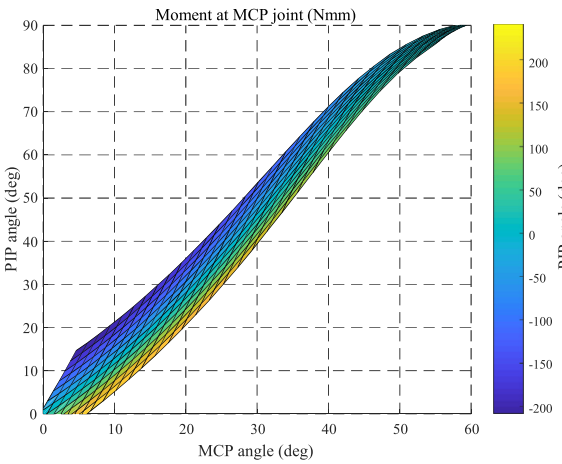

(d) Moment at MCP joint

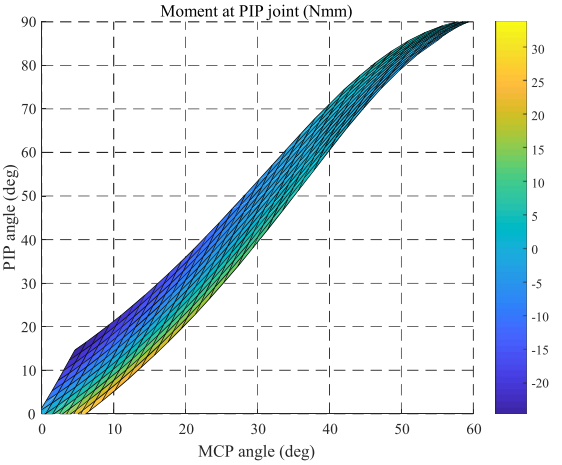

(e) Moment at PIP joint

Fig. 10. Force distribution analysis.

Fig. 11. Prototype of the proposed hand exoskeleton system.

We calculated the sensitivity of the moment to the cross-sectional area of the link, as shown in Fig. 10(b) and (c). This graph shows the sensitivity of the MCP and PIP joint moments when the cross-sectional area of the selected link varies from 9 mm^2 to 36 mm^2 while that of other links are constant as 9 mm^2. The joint moments were affected by only links 2-4. In particular, the moment of the PIP joint decreases dramatically as the cross-sectional area of link 3 increases and that of link 4 decreases. The reason is that the inertia of the structure according to the cross-sectional area and the length of the link plays a significant role in the force distribution and the link 3 and 4 are longer than other links. As the link 3 becomes thicker, the inertia of the structure around MCP joint increases, which increases the moment transmitted to the MCP joint. Similarly, the moment transmitted to the PIP joint depends on the thickness of link 4. Thus, we made link 3 slim, while ensuring that it supports the system, and link 4 was made thicker while making sure not to increase the system size. We designed the finger structure to distribute the spring force to each joint by adjusting the cross-sectional area of each link.

The moments of the joints induced by the designed finger structure are shown in Fig. 10(d) and (e). These figures show the moment transmitted to the MCP and PIP joints when the spring is compressed or stretched in the available finger postures. The negative value means the joint moment in the extension direction and the positive value means the joint moment in the flexion direction. The transmitted moment is up to 230 Nmm for the MCP joint and up to 35 Nmm for the PIP joint. Since the middle phalanx is more bent than the proximal phalanx, the moment of the PIP joint is much smaller than that of the MCP joint.

4. Performance verification

4.1. Implementation of the hand exoskeleton system

We designed and manufactured a hand exoskeleton system for exercising hand flexion/extension, as shown in Fig. 11(a) and (b). The device was designed for exercising four fingers, excluding the thumb. The wearing part was designed to make four fingers move together like a mitten. The silicone layer was added to the wearing part to compensate the difference of the phalanx height because of various finger lengths. The system is actuated by a linear motor to ensure that its structure is simple and light in weight. We reduced the number of actuators and the complexity of the system by actuating the structures for four fingers with a single linear motor. We used an embedded potentiometer to measure the motor stroke length to estimate finger postures.

We installed a spring on the bent link to generate and deliver forces to guide the fingers. We calculated the guidance forces by measuring the deflection using a potentiometer attached to the top of the spring case. We expect the distributed moments to be consistent with the results of the FEM analysis.

We used a compact and light linear motor as the actuator (L12-P, Actuonix, Canada), and used 3D printing to fabricate the links in the exoskeleton. For ease of wearing, we used Velcro and rubber bands around the palm and attached adjustable silicone bands to the finger phalanges. The dimensions of the device are $120 \times 195 \times 78$ mm, and the weight including the motor, is 156 g.

4.2. Finger motions wearing the hand exoskeleton

We verified the finger motions generated by the exoskeleton structure, by asking a non-impaired user to wear the device with a relaxed hand and follow the device as the actuator moved. The data for the user are summarized in Table I. We designed the exoskeleton structure for the user by following the proposed design process. Fig. 12 shows the experimental setup used to measure the motions of the finger joints. We attached markers to the structure and tracked the movements using a motion capture system. We calculated the finger joint angles of the exoskeleton by analyzing the movement of markers.

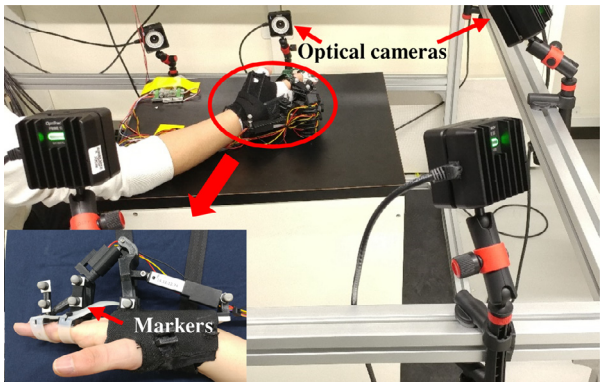

Fig. 12. Experimental setup.

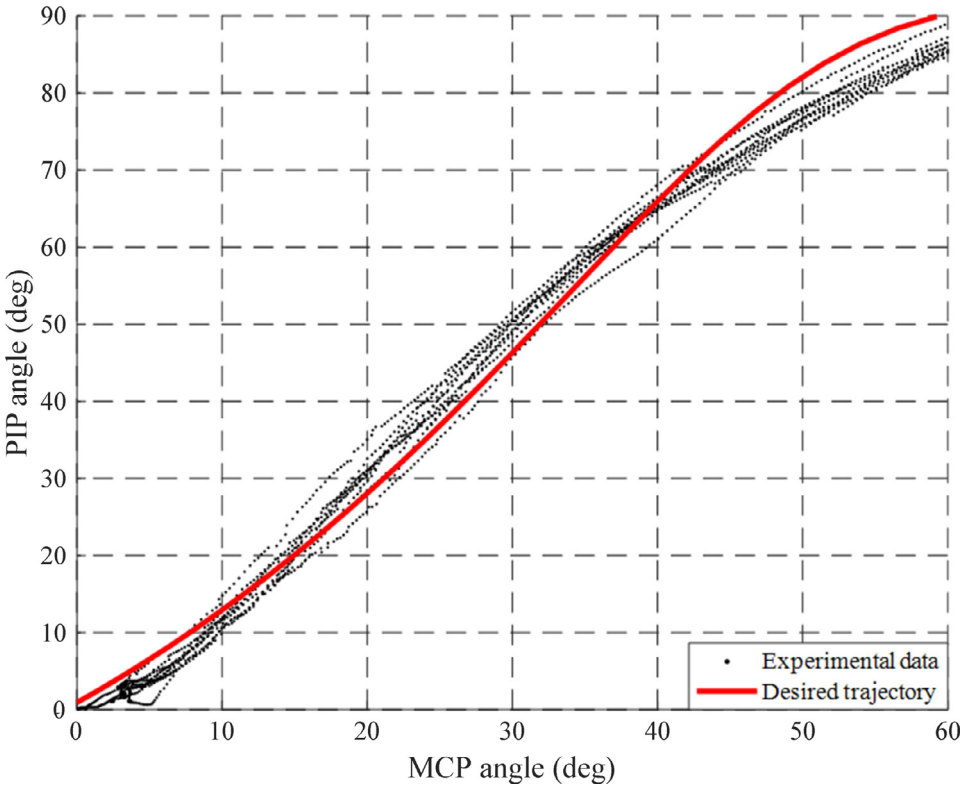

Fig. 13. Finger joint angles induced by the proposed device.

Fig. 13 shows the finger joint angles traversed by the user as they followed the movement of the exoskeleton. The red dots are the user's finger joint angles, and the solid line is the desired trajectory of the device. The user's joint angles were similar to the desired trajectory, with maximum deviations of 5°. This means that the hand rehabilitation device effectively guides the natural flexion/extension motions of the fingers along the desired trajectory.

4.3. Force distribution experiment

We validated the joint moments calculated by the FEM analysis by fabricating an artificial hand structure and making appropriate measurements. Fig. 14 shows the artificial hand with the finger structure. When a linear motor has a constant motor stroke and the spring is at its normal length, the posture of the artificial hand shows the desired posture according to the design in Section 3.2, so no moment was applied to MCP and PIP joints. The spring was activated, and it applied moments to the joints as the angles of the finger joints deviated from the desired posture. We ensured that the angles of the joints on the artificial finger remained deviated by calculating the finger angles corresponding to compressing or

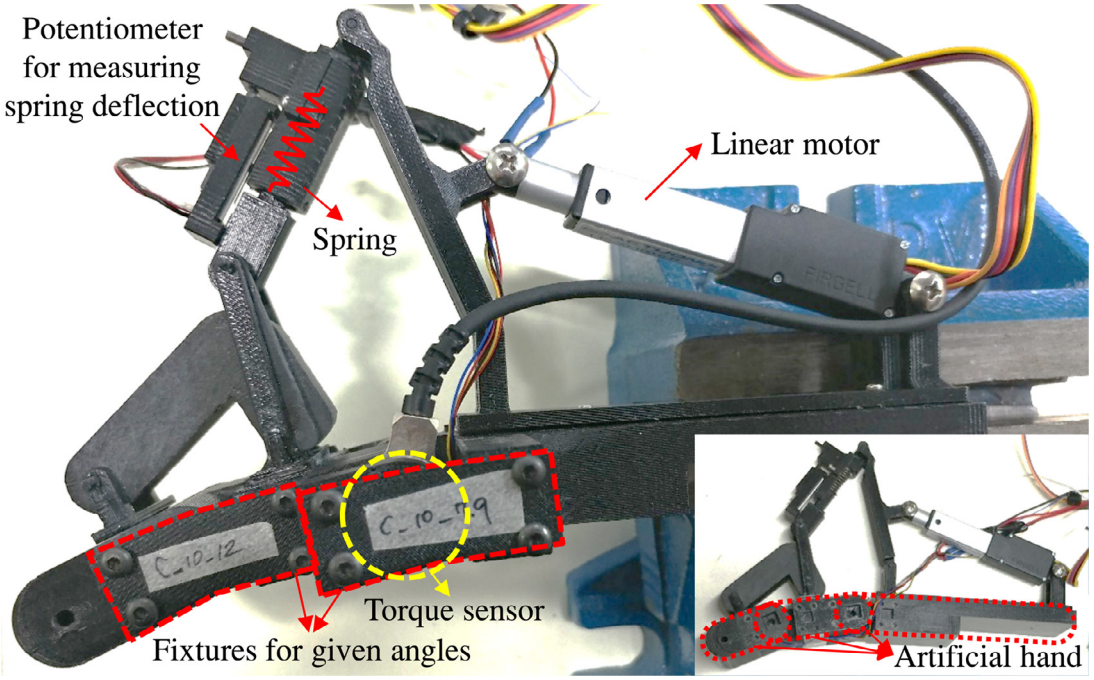

Fig. 14. Experimental setup.

Table 4
Force distribution experiment.

Spring condition	Desired posture (°)		Given posture (°)		Joint moment (Nmm)			
					FEM		Experiment	
	MCP	PIP	MCP	PIP	MCP	PIP	MCP	PIP
4 mm stretched (12 N)	8.1	10.4	12.7	25.0	190.2	19.4	183.7	14.4
	16.7	22.7	21.2	37.9	162.9	12.8	154.8	10.6
	25.8	38.4	30.2	53.8	123.6	5.3	117.1	4.2
4 mm compressed (12 N)	16.7	22.7	12.0	7.9	−219.3	−27.8	−214.1	−24.0
	25.8	38.4	21.3	22.9	−194.1	−20.4	−174.3	−17.2
	35.7	57.6	31.4	42.2	−152.8	−10.7	−143.1	−7.1

stretching the spring by 4 mm, then attaching fixtures that realized the calculated angles on the artificial hand. The spring deflected the artificial hand to guide the deviation in posture. We then measured the moments transmitted to the joints using a torque sensor.

Table 4 shows the joint moments according to the results of the FEM analysis and the experimentally measured values. These results are in good agreement. Thus, we validated the design process used to adjust the cross-sections of links. We also confirmed that the designed moment was transmitted to the user's hand.

5. Conclusion

In this paper, we proposed a portable and spring-guided hand exoskeleton system for exercising flexion/extension of the fingers. The design of the exoskeleton, in which two linkages were combined, was proposed for underactuation. We investigated the general finger motions of several subjects by conducting grasping experiments. The design of the linkage structure was optimized based on the users finger, joint ROM, and the obtained general finger motions. The spring, attached to the finger structure, generates the guidance force to the fingers; the magnitude of this force depends on the fingers deviation from the desired posture. We conducted FEM analysis to analyze that the transmitted moment to MCP and PIP joints. The prototype of the wearable hand rehabilitation device was built with consideration of its wearability and its performance was experimentally verified. The results of our measurements of the finger motion confirmed that the hand rehabilitation device guided the hand in a manner that would help the user to perform general flexion/extension motions. We also carried out a force distribution experiment to verify that the moments generated were similar to the results of the FEM analysis. Thus, the system successfully guided the users fingers along the desired trajectory and distributed the expected moments to the joints.

The research for the thumb was excluded in this paper because of its complex structure and wide ROM. As future work, the system including the structure for the thumb exercise will be developed for full exercise of all fingers.

Acknowledgments

This work was supported by the Global Frontier R&D Program on < Human-centered Interaction for Coexistence > funded by the National Research Foundation of Korea grant funded by the Korean Government (MSIP) (No. NRF-2012M3A6A3056354), the National Research Foundation of Korea Grant funded by the Korean Government (MSIT) (No. NRF-2016R1A5A1938472) and Institute for Information & communications Technology Promotion (IITP) grant funded by the Korea Government (MSIP) (No. 2017000910001100, Development of multi-material 3D printing technologies for flexible motion detection and control sensor modules). Preliminary version of this paper was presented at the IEEE International Conference on Rehabilitation Robotics (ICORR) 2017 [29].

Supplementary material

Supplementary material associated with this article can be found, in the online version, at doi:10.1016/j.mechmachtheory.2019.02.004.

References

[1] M.M. Pinter, M. Brainin, Rehabilitation after stroke in older people, Maturitas 71 (2012) 104–108, doi:10.1016/j.maturitas.2011.11.011.
[2] S. Bagg, A.P. Pombo, W. Hopman, Effect of age on functional outcomes after stroke rehabilitation, Stroke 33 (2002) 179–185.
[3] P. Langhorne, J. Bernhardt, G. Kwakkel, Stroke rehabilitation, Lancet 377 (2011) 1693–1702, doi:10.1016/S0140-6736(11)60325-5.
[4] X.L. Hu, K. yu Tong, R. Song, X.J. Zheng, W.W.F. Leung, A comparison between electromyography-driven robot and passive motion device on wrist rehabilitation for chronic stroke, Neurorehabil. Neural Repair 23 (2009) 837–846, doi:10.1177/1545968309338191.
[5] A.J. Szameitat, S. Shen, A. Conforto, A. Sterr, Cortical activation during executed, imagined, observed, and passive wrist movements in healthy volunteers and stroke patients, NeuroImage 62 (2012) 266–280, doi:10.1016/j.neuroimage.2012.05.009.
[6] D. Dirette, J. Hinojosa, Effects of continuous passive motion on the edematous hands of two persons with flaccid hemiplegia, Am. J. Occup. Therapy 48 (1994) 403–409.
[7] M.L. Giudice, Effects of continuous passive motion and elevation on hand edema, Am. J. Occup. Therapy 44 (1990) 914–921.
[8] S.W. O'Driscoll, N.J. Giori, Continuous passive motion (cpm) : theory and principles of clinical application, J. Rehabil. Res. Dev. 37 (2000) 179–188.
[9] M. R. Buschfort, J. Brocke, A. Hess, C. Werner, A. Waldner, S. Hesse, Arm studio to intensify upper limb rehabilitation after stroke: concept, acceptance, utilization and preliminary clinical results, J. Rehabil. Med. 42 (2010) 310–314, doi:10.2340/16501977-0517.
[10] G.B. Prange, M.J.A. Jannink, C.G.M. Groothuis-Oudshoorn, H.J. Hermens, M.J. IJzerman, Systematic review of the effect of robot-aided therapy on recovery of the hemiparetic arm after stroke, J. Rehabil. Res. Dev. 43 (2006) 171–184, doi:10.1682/JRRD.2005.04.0076.
[11] H. Krebs, J. Palazzolo, L. Dipietro, M.F.J. Krol, K. Rannekleiv, B. Volpe, N. Hogan, Rehabilitation robotics: performance-based progressive robot-assisted therapy, Auton. Robots 15 (2003) 7–20, doi:10.1023/A:1024494031.
[12] M. Hillman, 2 rehabilitation robotics from past to present a historical perspective, Adv. Rehabil. Rob., 2006.
[13] M.A. Rahmana, A. Al-Jumaily, Design and development of a hand exoskeleton for rehabilitation following stroke, in: International Symposium on Robotics and Intelligent Sensors (IRIS), 2012, pp. 1028–1034, doi:10.1016/j.proeng.2012.07.279.
[14] F. Zhang, L. Hua, Y. Fu, H. Chen, S. Wang, Design and development of a hand exoskeleton for rehabilitation of hand injuries, Mech. Mach. Theory 73 (2014) 103–116, doi:10.1016/j.mechmachtheory.2013.10.015.
[15] J. Iqbal, H. Khan, N.G. Tsagarakis, D.G. Caldwell, A novel exoskeleton robotic system for hand rehabilitation conceptualization to prototyping, Biocybern. Biomed. Eng. 34 (2014) 79–89, doi:10.1016/j.bbe.2014.01.003.
[16] F. Zhang, X. Wang, Y. Fu, S.K. Agrawal, A human-robot interaction modeling approach for hand rehabilitation exoskeleton using biomechanical technique, in: International Conference on Intelligent Robots and Systems (IROS), 2015, pp. 5593–5598, doi:10.1109/IROS.2015.7354170.
[17] C.N. Schabowsky, S.B. Godfrey, R.J. Holley, P.S. Lum, Development and pilot testing of hexorr: hand exoskeleton rehabilitation robot, J. Neuroeng. Rehabil. 7 (2010), doi:10.1186/1743-0003-7-36.
[18] Y. Yun, P. Agarwal, J. Fox, K.E. Madden, A.D. Deshpande, Accurate torque control of finger joints with ut hand exoskeleton through bowden cable sea, in: International Conference on Intelligent Robots and Systems (IROS), 2016, pp. 390–397, doi:10.1109/IROS.2016.7759084.
[19] T. Worsnopp, M. Peshkin, J. Colgate, D. Kamper, An actuated finger exoskeleton for hand rehabilitation following stroke, in: IEEE International Conference on Rehabilitation Robotics (ICORR), 2007, pp. 896–901, doi:10.1109/ICORR.2007.4428530.
[20] S. Ueki, H. Kawasaki, S. Ito, Y. Nishimoto, M. Abe, T. Aoki, Y. Ishigure, T. Ojika, T. Mouri, Development of a hand-assist robot with multi-degrees-of-freedom for rehabilitation therapy, IEEE/ASME Trans. Mechatron. 17 (2012) 136–146, doi:10.1109/TMECH.2010.2090353.
[21] D.G. Kamper, E.G. Cruz, M. Siegel, Stereotypical fingertip trajectories during grasp, J. Neurophysiol. 90 (2003) 3702–3710.
[22] R. Conti, E. Meli, A. Ridolfi, A novel kinematic architecture for portable hand exoskeletons, Mechatronics 35 (2016) 192–207, doi:10.1016/j.mechatronics.2016.03.002.
[23] J. Yang, H. Xie, J.S. School, A novel motion-coupling design for a jointless tendon-driven finger exoskeleton for rehabilitation, Mech. Mach. Theory 99 (2016) 83–102, doi:10.1016/j.mechmachtheory.2015.12.010.
[24] D. Neumann, E. Rowan, Kinesiology of the Musculoskeletal System: Foundations for Physical Rehabilitation, Mosby Philadelphia, 2002.
[25] J. Li, R. Zheng, Y. Zhang, J. Yao, Ihandrehab: an interactive hand exoskeleton for active and passive rehabilitation, in: International Conference on Rehabilitation Robotics (ICORR), 2011, pp. 1–6, doi:10.1109/ICORR.2011.5975387.
[26] N. Hogan, Impedance control: an approach to manipulation. parts i, ii, and iii, J. Dyn. Syst. Meas. Control 107 (1985) 1–24, doi:10.1115/1.3140713.
[27] J. Bae, M. Tomizuka, A gait rehabilitation strategy inspired by an iterative learning algorithm, Mechatronics 22 (2012) 213–221.
[28] N. Kim, B.V. Sankar, Introduction to Finite Element Analysis and Design, John Wiley and Sons, 2009.
[29] I. Jo, J. Lee, Y. Park, J. Bae, Design of a wearable hand exoskeleton for exercising flexion/extension of the fingers, in: IEEE Proceeding on Rehabilitation Robotics (ICORR), 2017, pp. 1615–1620.